Chapter 3

Probing of Incomplete Fusion: Forward Recoil Range Distribution Measurements

Relative contribution of complete fusion (CF) and incomplete fusion (ICF) channels observed in heavy ion induced reaction have been deduced from the analysis of measured excitation functions (EFs) taking care of complete fusion code PACE-2 and it has been shown in the previous Chapter that with increase in the incident projectile energy, the ICF becomes more and more dominant. On the other hand, the measurement of forward recoil range distribution (FRRD) is one of the straight forward qualitative methods, which furnish the information about the relative contribution of CF and ICF processes, which depend upon the linear momentum transfer from projectile to target nucleus. In case of CF process, entire projectile is captured by the target nucleus, and hence maximum linear momentum transfer is expected. In case of ICF process, a part of the projectile is captured by the target nucleus which leads to partial linear momentum transfer from projectile to target nucleus and rest of the projectile moves in the forward direction as a spectator. Hence, the reaction products (radio-nuclides) formed via CF will show a longer range in the stopping medium as compared to ICF reaction products, where partial linear momentum transfer takes place. Therefore, the measurement of forward recoil range distributions (FRRDs) may be used as a probe to investigate the partial fusion of the projectile with the target in ICF process.

Present understanding of ICF dynamics is not fully explored and is limited to few projectile and target combination systems. In order to have a better understanding of fusion incompleteness and to give a complement to excitation function (EF)

measurements, presented in Chapter 2, measurement of forward recoil range distributions (FRRDs) of radio-nuclides populated via CF and/or ICF in ^{20}Ne + ^{159}Tb system at ~ 164 MeV energy and in ^{16}O + ^{156}Gd system at three different projectile energies i.e., at ~ 72, ~ 82 and ~ 93 MeV, have been done. An attempt has been made to separate the relative contributions of CF and ICF from experimentally measured forward RRDs for the above said systems. In the present work recoil-catcher activation technique, followed by off-line γ–ray spectroscopy, has been used.

3.1 Experimental Details

The experiments have been performed using energetic ^{20}Ne and ^{16}O- ion beam delivered from Variable Energy Cyclotron, at Variable Energy Cyclotron Centre (VECC), Kolkata, India and 15UD-Pelletron Accelerator of Inter-University Accelerator Centre (IUAC), New Delhi, India. In order to study the CF and ICF reaction dynamics, forward recoil range distributions for the residues produced in ^{20}Ne + ^{159}Tb system at ~ 164 MeV projectile energy and in ^{16}O + ^{156}Gd system at three different projectile energies ~ 72, ~ 82 and ~ 93 MeV, have been measured. Although methodological details are somewhat similar to those already given in Chapter 2, for a quick reference, a brief description of sample preparation, irradiation of the sample and post irradiation analysis is given in the following sub-sections.

3.1.1 Target preparation and irradiations

In the forward recoil range distribution (FRRD) measurements of the produced evaporation residues (ERs) in heavy-ion interactions, targets and catcher foils were prepared at Target Laboratory of VECC, Kolkata and IUAC, New Delhi. The self-supporting isotopically pure natural sample of ^{159}Tb of thickness ~ 0.73 mg/cm^2 (Abundance =100%) and stack of thin Al-catcher foils (used to trap recoiling residues produced by ^{159} Tb target) of thicknesses lying between ~71-95 μg/cm^2 have been prepared by ultra high vacuum evaporation technique at VECC, Kolkata. While, three

enriched targets of ^{156}Gd (abundance ≈ 94.8%) of thicknesses ~ 0.59, ~ 0.83 and ~ 0.77 mg/cm^2 were deposited by employing electro-deposition technique on Al-foils (used as backing) of thicknesses ~1.14, 1.20 and 0.98 mg/cm^2 respectively, prepared by rolling technique, at IUAC, New Delhi. Three stacks of thin Al-catcher foils (used to trap recoiling residues produced by ^{156}Gd target) of thicknesses lying between ~ 40-87 μg/cm^2, have been prepared by ultra-high vacuum evaporation technique at IUAC, New Delhi. The effective projectile energy in ^{156}Gd target has been estimated by calculating energy loss in its Al-backing. The thickness of each target and individual Al-catcher foils has been estimated by α-transmission method as discussed in the Chapter 2.

The irradiations of ^{159}Tb target along with catchers have been performed using ^{20}Ne - ion beam in a specially designed vacuum chamber at VECC, Kolkata at projectile energy ~ 165 MeV and of ^{156}Gd along with catchers using ^{16}O- ion beam in General Purpose Scattering Chamber (GPSC) at IUAC, New Delhi at three different projectile energies i.e., ~ 76, 86 and 96 MeV.

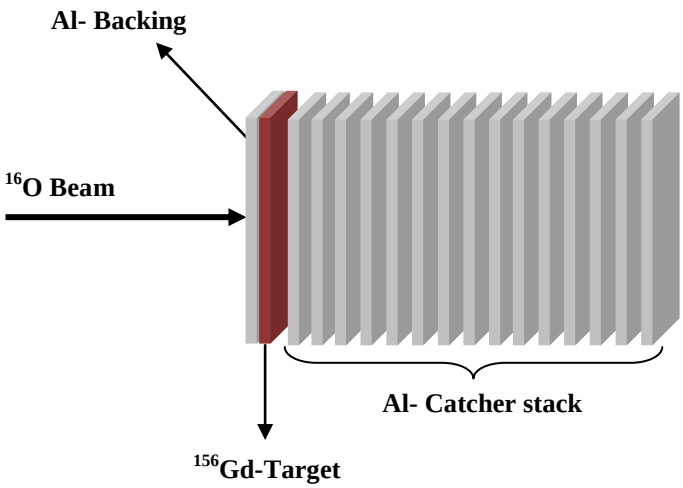

Fig. 3.1: Typical arrangement of target ^{156}Gd with Al-catcher foils used for forward recoil range distribution (FRRD) measurement.

Table 3.1: List of Al-catcher foil thicknesses used in FRRD measurements, for ^{20}Ne + ^{159}Tb and ^{16}O + ^{156}Gd systems at different projectile energies.

S. No.	^{20}Ne + ^{159}Tb Catcher thickness in ($\mu g/cm^2$) used at energy ~164 MeV	^{16}O + ^{156}Gd Catcher thickness in ($\mu g/cm^2$) used at energy ~72 MeV	~82 MeV	~93 MeV
1.	95.3	43.0	43.0	42.8
2.	90.0	47.9	43.0	40.3
3.	97.0	59.6	43.1	45.7
4.	77.0	56.0	46.4	39.2
5.	78.4	49.6	59.5	43.2
6.	82.8	63.2	50.0	43.2
7.	71.2	69.5	84.4	46.6
8.	78.4	69.5	87.7	46.6
9.	78.4	78.9	43.0	43.2
10.	78.4	53.9	43.1	40.0
11.	78.4	53.0	40.0	43.0
12.	78.0	50.0	40.0	46.3
13.	78.0	48.0	42.0	67.0
14.	78.0	43.0	43.0	60.2
15.	---	46.4	43.0	54.7
16.	---	---	40.0	48.6
17.	---	---	---	52.8
18.	---	---	---	50.0
19.	---	---	---	50.0

Stacks of Al catcher foils were placed just after the respective targets, so that residues populated via CF and/or ICF may be trapped at various Al-catcher foil thicknesses. A typical target-catcher foils arrangement used for the FRRDs measurement of ^{156}Gd is shown in Fig. 3.1. Thicknesses of Al-catcher foils, used in each FRRD measurements, for both the systems, are listed in Table 3.1. For the measurement of FRRD, it is quite essential that recoiling residues may move in the forward cone or towards the Al-catcher foils placed in the forward direction. However, for the FRRD measurement with ^{156}Gd targets, which were deposited on Al-backings, the mounting was done in such away that Al-backing faced the ^{16}O-ion beam. The actual projectile energy on target has been estimated by calculating the energy loss in Al-backing of the target ^{156}Gd. The incident beam energies in three separate irradiations for FRRD measurements were 76, 86, and 96 MeV. After some energy loss in Al-backing, the energies in the three separate irradiations of ^{156}Gd, were estimated to be ~ 72, ~ 82 and ~93 MeV. The irradiations have been carried out using ^{20}Ne- ion beam on ^{159}Tb for ~ 21 hrs at the beam current ~ 34 nA, while, using ^{16}O-ion beam on ^{156}Gd for ~ 12 hrs (at ~72 MeV) , ~ 13 hrs (at ~ 82 MeV) and ~ 15 hrs (at ~ 93 MeV) with beam currents ~ 48, 60 and 15nA respectively.

3.1.2 Post irradiation analysis and identification of ERs

After the irradiation, target-catcher assemble was taken out from the scattering chamber and target-catcher foils were dismantled to count the activities induced in the individual irradiated catcher foils. The evaporation residues (ERs) populated via CF and/or ICF process are expected to be trapped at different catcher foil thicknesses, depending upon the degree of linear momentum transfer associated with the mode of formation. The residual γ-activity induced in each catcher-foil counted separately with increasing time using pre-calibrated high resolution HPGe detector coupled to a PC based data acquisition system equipped with Software MAESTRO [1] at VECC, Kolkata and FREEDOM [2] at IUAC, New Delhi, which has already been discussed in Section

2.1.3 of Chapter 2. Thus, the induced γ-activity has been used to measure the production probability of the ERs. The γ-ray spectrum of each foil has been recorded with increasing times and decay curve analysis has been done to ensure the production of the identified residues. The measured half-lives of each residue were found to be in agreement with the literature values. Typical γ-ray energy spectra recorded after irradiation of ^{159}Tb and ^{156}Gd targets with ^{20}Ne and ^{16}O-ion beam energies ~ 164 and ~ 93 MeV respectively are displayed in Fig. 3.2 and Fig. 3.3.

The production cross-sections of ERs populated for presently studied systems have been measured, using expression (2.3), given in Chapter 2.All the spectroscopic data used for measured cross-section calculations were taken from Ref. [3, 4]. The

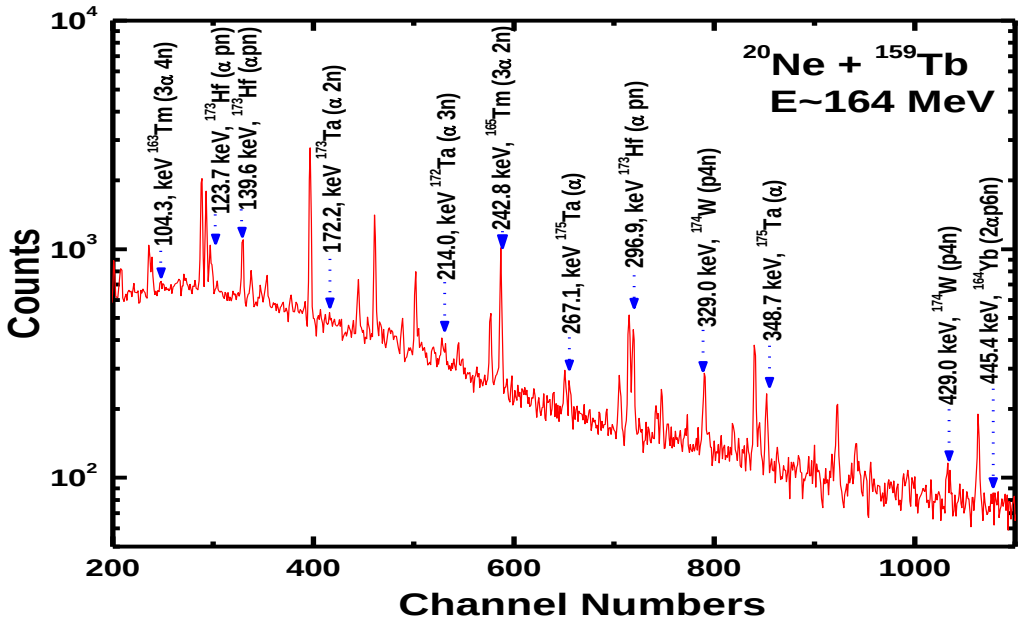

Fig. 3.2: Typical γ-ray energy spectrum of ^{159}Tb sample irradiated by ^{20}Ne-ion beam at ~ 164 MeV energy, between 200-1100 channels. The peaks have been assigned to different reaction products populated via CF and /or ICF.

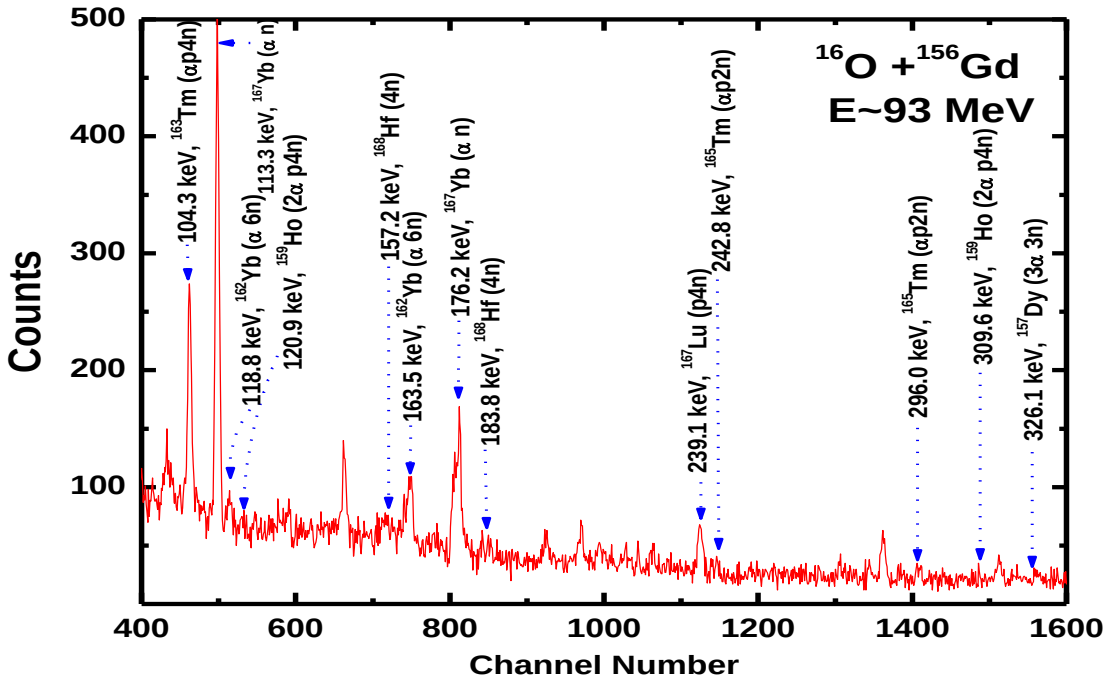

Fig. 3.3: Typical γ-ray energy spectrum of ^{156}Gd sample irradiated by ^{16}O ion beam at ~93 MeV energy, between 400-1600 channels. The peaks have been assigned to different reaction products populated via CF and /or ICF.

measured cross-section of the residue in each catcher foils was divided by its individual thickness to get the normalized yield [mb/**(**mg/cm^2)]. The resulting normalized yields of the different reaction products have been plotted as function of cumulative catcher thickness to obtain differential recoil range distributions of the populated residues. In the present work, forward recoil range distributions of nine ERs ^{174}W, ^{175}Ta, ^{173}Ta, ^{172}Ta, ^{173}Hf, ^{164}Yb, ^{166}Tm, ^{165}Tm, ^{163}Tm populated in ^{20}Ne + ^{159}Tb system at ~ 164 MeV, while eight ERs; ^{168}Hf, ^{167}Lu, ^{167}Yb, ^{162}Yb, ^{165}Tm, ^{163}Tm, ^{159}Ho^{g} and ^{157}Dy populated in ^{16}O + ^{156}Gd system at three different projectile energies ~ 72, 82 and 93 MeV, have been measured.

3.2 Results and Discussion

3.2.1 Forward recoil range distributions: ^{20}Ne + ^{159}Tb system

In order to get the information about linear momentum transfer (LMT) components associated with complete fusion (CF) and/or incomplete fusion (ICF) reaction products, forward recoil range distributions (FRRDs) for nine radio-nuclides ^{174}W (p4n), ^{175}Ta (α), ^{173}Ta (α2n), ^{172}Ta (α3n), ^{173}Hf (αpn), ^{164}Yb (2αp6n), ^{166}Tm (3αn), ^{165}Tm (3α2n) and ^{163}Tm (3α4n) populated in CF and/or ICF have been measured at projectile energy ~ 164 MeV. As such the normalized yields for these residues to obtain FRRDs have also been generated as a function of cumulative catcher thickness for each residue. These are listed in Tables 3.2 and 3.3 and displayed in Figs. 3.4-3.6. The FRRDs of ER ^{174}W is shown in Fig. 3.4(a). The evaporation residue ^{174}W is produced by emission of 1 proton and 4 neutrons from the composite system ^{179}Re*, populated in the fusion of ^{20}Ne with ^{159}Tb. As it can be observed from the Fig. 3.4(a) that FRRD of ^{174}W shows single Gaussian peak at cumulative thickness ~ 985 μg/cm^2, corresponding to full momentum transfer from projectile to target. The experimentally measured most probable range of ^{174}W reaction product is found to be in good agreement with theoretically calculated range ~ 970 μg/cm^2, using code SRIM08 [5], which clearly shows that the product ^{174}W is formed via CF of ^{20}Ne with ^{159}Tb. Comparisons of measured and theoretical ranges are given in Table 3.4.

The measured FRRD of the residues ^{175}Ta and ^{173}Ta, populated in break-up α-emission channel, are shown in Figs. 3.4 (b)-(c). One may observe from these figures that these residues give single Gaussian recoil peak at cumulative catcher thickness ~ 924 μg/cm^2 and 913 μg/cm^2 respectively, which corresponds to the residues produced predominantly through ICF of projectile ^{20}Ne i.e., in fusion of the fragment ^{16}O (produced in the break-up of the projectile ^{20}Ne into ^{16}O and ^{4}He (α)) with target nucleus ^{159}Tb, forming incompletely fused composite system ^{175}Ta* in the excited state.

Table 3.2 Experimentally measured forward recoil range distributions (FRRDs) of the residues ^{174}W, ^{175}Ta, ^{173}Ta, ^{172}Ta and ^{173}Hf produced in ^{20}Ne + ^{159}Tb reactions at ~164 MeV energy.

Cumulative thickness (μg/cm^2)	**Recoil range distributions (yields) of the residues measured in [mb/(mg/cm^2)]**				
	^{174}W	**^{175}Ta**	**^{173}Ta**	**^{172}Ta**	**^{173}Hf**
95.3	1.6	60.0	162.0	178.0	298.0
185.3	2.0	65.0	169.0	189.0	289.0
282.3	5.3	59.0	167.0	185.0	290.0
359.3	7.4	67.5	173.0	180.0	296.0
437.7	7.2	65.0	164.0	175.0	292.0
520.5	7.5	61.0	159.4	177.0	297.0
591.7	19.6	73.0	172.0	189.0	289.0
670.1	29.4	67.6	159.4	177.0	282.0
748.5	64.3	69.0	172.0	229.0	312.0
826.9	557	126.2	241.0	328.0	454.0
905.3	1651	165.8	326.5	365.0	507.0
983.3	1934	154.0	257.6	285.0	462.0
1061.3	1620	101.0	193.0	235.0	345.0
1139.3	760	76.5	175.0	189.0	295.0

In its de-excitation by 2 neutrons, residue ^{173}Ta is produced. However, un-fused 'fast' α-particle moves in forward direction. As such, production of these residues are observed in ICF of the projectile and a partial linear momentum transfer (LMT) takes from projectile to the target. Most probable recoil peaks at measured cumulative catcher

thicknesses for residues ^{175}Ta and ^{173}Ta are in agreement with theoretically calculated ranges.

Table 3.3 Experimentally measured forward recoil range distributions (FRRDs) of the residues ^{164}Yb, ^{166}Tm, ^{165}Tm and ^{163}Tm produced in ^{20}Ne + ^{159}Tb reactions at ~164 MeV energy.

Cumulative thickness ($\mu g/cm^2$)	**Recoil range distributions (yields) of the residues measured in [mb/(mg/cm^2)]**			
	^{164}Yb	**^{166}Tm**	**^{165}Tm**	**^{163}Tm**
95.3	22.0	7.5	16.0	31.0
185.3	25.0	8.3	18.0	26.0
282.3	30.0	10.1	17.0	30.0
359.3	32.0	36.2	23.0	61.0
437.7	29.0	45.0	34.0	71.0
520.5	30.0	40.0	29.0	65.0
591.7	47.0	46.0	31.0	71.0
670.1	81.0	65.0	40.0	88.0
748.5	85.0	51.0	34.0	69.0
826.9	89.0	53.0	38.0	74.0
905.3	114.0	62.6	45.0	90.0
983.3	89.0	36.0	29.0	65.0
1061.3	45.0	7.0	16.0	30.0
1139.3	29.0	8.0	16.2	31.0

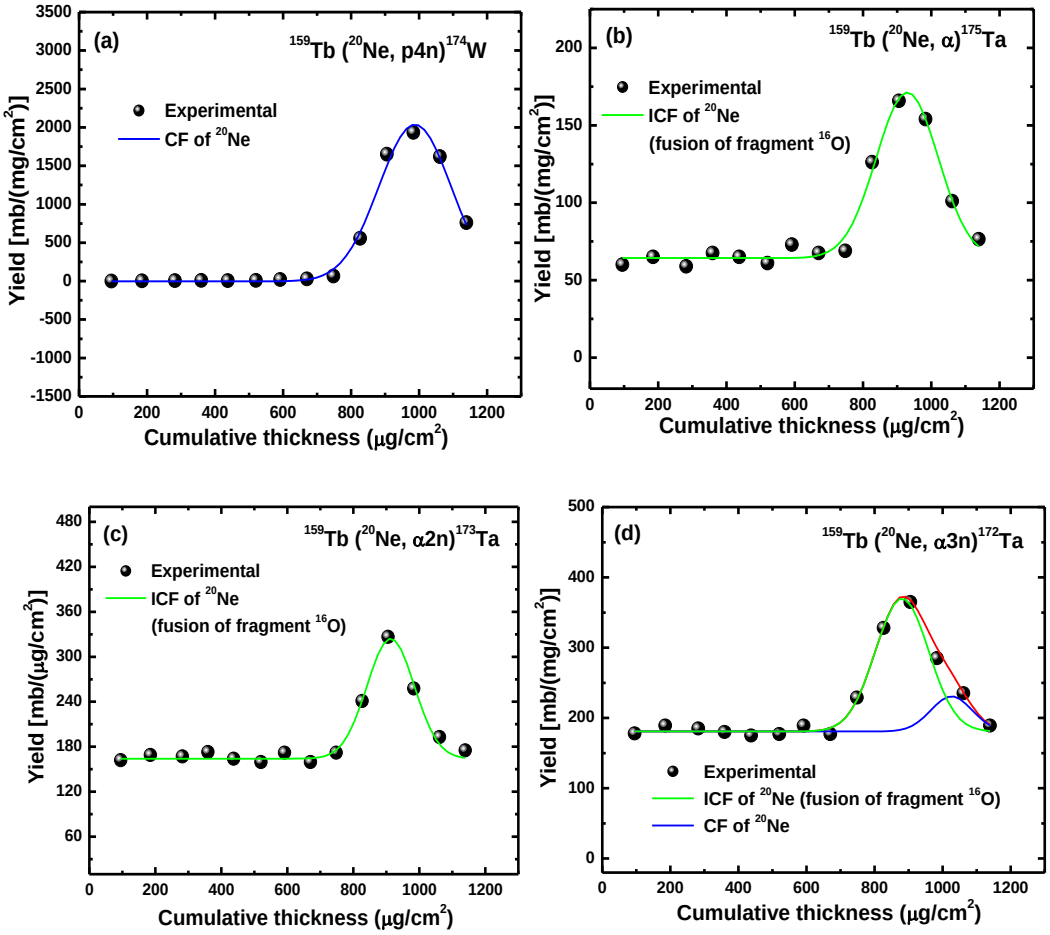

Fig. 3.4: The experimentally measured forward recoil range distributions (FRRDs) of evaporation residues ^{174}W, ^{175}Ta, ^{173}Ta and ^{172}Ta, produced via CF and/or ICF, for ^{20}Ne + ^{159}Tb system at energy, E ~ 164 MeV.

The forward recoil range distribution of residue ^{172}Ta shows two peaks structure as shown in Fig. 3.4 (d). As can be observed from this figure, the residues ^{172}Ta may be formed via CF as well ICF of ^{20}Ne with ^{159}Tb. In case of CF, the composite system ^{179}Re* is formed, which may decay via statistical emission of 1 α-particle and 3 neutrons

leaving behind the residue ^{172}Ta. This residue may also be populated via ICF of the projectile, where as the fragment ^{16}O (in the projectile break-up) fuses with target nucleus ^{159}Tb, forming an incompletely composite system ^{175}Ta*, which may decay by the emission of 3 neutrons leaving behind the above residue. In the CF of the projectile, full linear momentum transfer (LMT) takes place and peak is observed at cumulative catcher thickness ~ 1009 μg/cm^2, while in ICF of the projectile, since a partial linear momentum is transferred, the peak is observed at a smaller distance in the catcher medium, ~ 904 μg/cm^2. The measured mean recoil ranges are in close agreement with the theoretical ranges, ~970 and ~ 916 μg/cm^2 respectively, calculated using code SRIM08 [5].

Looking over the FRRD of the residue ^{173}Hf, it again shows single Gaussian peak is observed as shown in Fig.3.5(a) at cumulative catcher thickness ~ 912 μg/cm^2, which corresponds to the range of ICF of the projectile (in the fusion of fragment ^{16}O with target). As such, residue ^{173}Hf is also expected to be produced in the ICF of the projectile, where as partial momentum transfer takes place. Here again measured range is also in agreement with its theoretical range, estimated using code SRIM08 [5]. The absence of the CF channel peak indicates that residue ^{175}Ta, ^{173}Ta and ^{173}Hf are predominantly populated through the ICF of ^{20}Ne with ^{159}Tb.

Further moreover, in case of 2α-emission product ^{164}Yb, forward RRD shows a composite structure which is resolved to get two recoil peaks at cumulative thicknesses ~ 907 and ~ 683 μg/cm^2 as displayed in Fig. 3.5 (b). The peak observed at higher range corresponds to the ICF of ^{20}Ne i.e., fusion of fragment ^{16}O [if ^{20}Ne breaks-up into ^{16}O and ^{4}He (α)] with ^{159}Tb. The second recoil peak observed at lower range corresponds to ICF of the projectile in the fusion of fragment ^{12}C [if ^{20}Ne breaks-up into ^{12}C and ^{8}Be (2α)] with the target. It is obvious that the partial linear momentum transfer (LMT) in fusion of the fragment ^{16}O will be more than in fusion of fragment ^{12}C. The peak corresponding to expected mean recoil range (~970 μg/cm^2) of CF channel has not been observed. The absence of the CF channel peak indicates that the residue ^{164}Yb

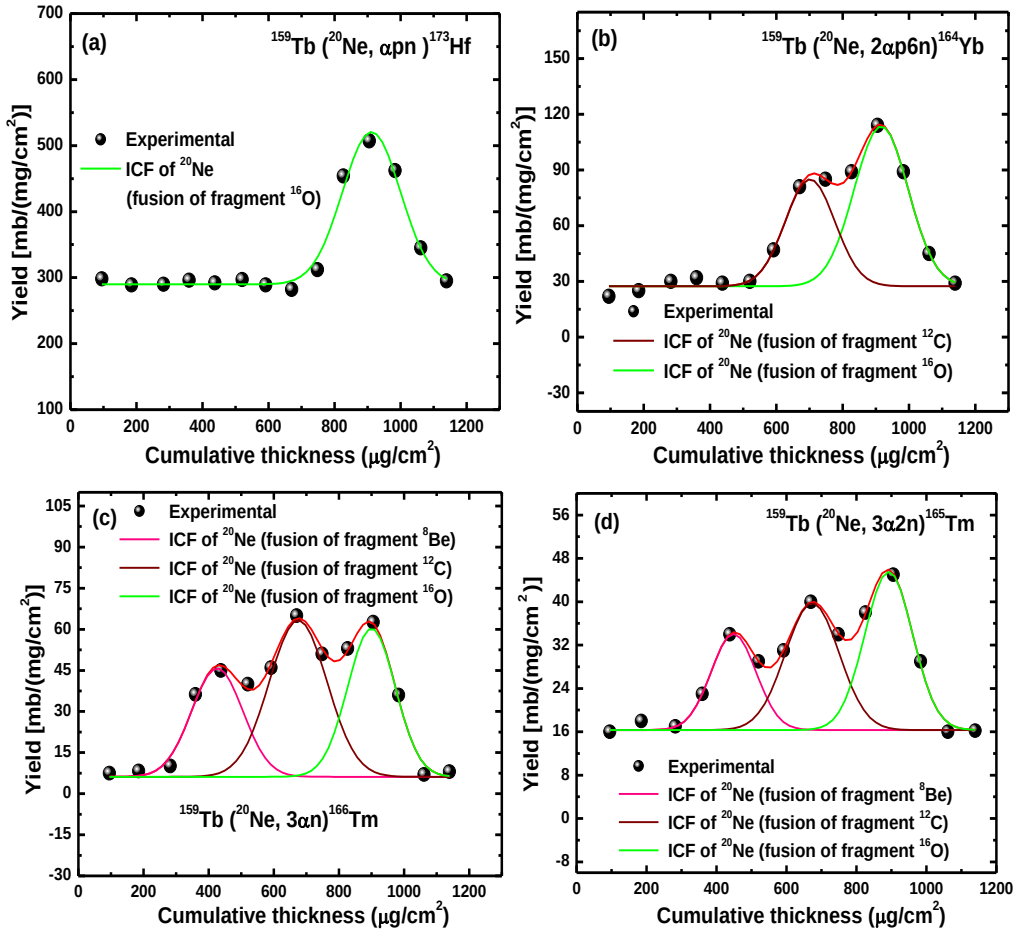

Fig. 3.5: The experimentally measured forward recoil range distributions (FRRDs) of evaporation residues ^{173}Hf, ^{164}Yb, ^{166}Tm and ^{165}Tm, produced via ICF, for ^{20}Ne + ^{159}Tb system at energy, E ~ 164 MeV.

predominantly produced through the ICF of ^{20}Ne with different degree of linear momentum transfer. The experimentally measured EFs of the residue ^{164}Yb showing negligible theoretical cross-section (obtained from PACE-2) may clearly indicate that the evaporation residue ^{164}Yb produced mainly through ICF reaction channels.

The observed forward RRDs for the evaporation residue ^{166}Tm produced in 3αn emission channel, shows three resolved peaks [shown in Figs. 3.5(c)] , associated with three different partial linear momentum transfer (LMT) components corresponding to mean cumulative catcher thicknesses ~ 905, ~ 658 and ~ 432 μg/cm^2. The observed mean recoil range at cumulative thickness ~ 905 μg/cm^2 is due to ICF of ^{20}Ne (i.e., fusion of fragment ^{16}O in the break-up of ^{20}Ne into ^{16}O and ^{4}He) with the target ^{159}Tb, the observed mean recoil range at thickness ~ 658 μg/cm^2 is due to ICF of ^{20}Ne with the target ^{159}Tb (where as fusion of fragment ^{12}C produced in the break-up of ^{20}Ne into ^{12}C and ^{8}Be takes place) and the observed mean recoil range at thickness ~ 432 μg/cm^2 is due to ICF of ^{20}Ne with the target ^{159}Tb (where as fusion of fragment ^{8}Be of the projectile ^{20}Ne in the break-up of ^{20}Ne into fragments ^{8}Be and ^{12}C takes place), have been observed. Absence of the peak corresponding to the CF channel indicates that the reaction predominantly goes through ICF channels only.

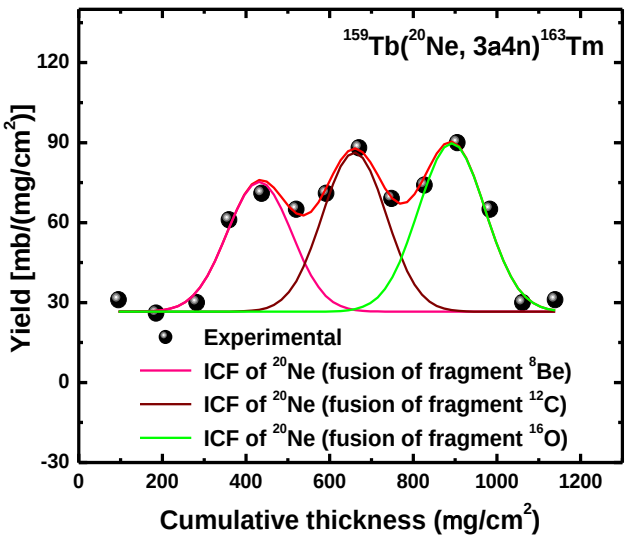

Fig. 3.6: The experimentally measured forward recoil range distribution (FRRD) of evaporation residue ^{163}Tm, produced via ICF, for ^{20}Ne + ^{159}Tb system at energy, E ~ 164 MeV.

The above descriptions clearly indicate that peaks appearing at different cumulative thickness in the stopping medium are related to different degrees of linear momentum transfer from projectile to the target.

As such, the recoil profiles of the residues ^{165} Tm and ^{163}Tm in Al-catchers, produced in 3α2n and 3α4n reaction channels also show three recoil Gaussian peaks, associated with three partial linear momentum transfer (LMT) components at three cumulative catcher thicknesses. In residue ^{165}Tm, as shown in Figs. 3.5 (d), three well resolved peaks are observed at ~ 906 , ~ 663 and ~ 448 μg/cm^2 while in ^{163}Tm , as shown in Fig. 3.6, peaks are observed at ~ 903 , ~ 656 and ~ 440 μg/cm^2 . As discussed above, these peaks are associated with ICF of projectile ^{20}Ne (i.e., in the fusion of fragment ^{16}O, fusion of fragment ^{12}C and fusion of fragment ^{8}Be respectively) with the target ^{159}Tb. Observation of no peak at CF recoil range, indicates that no full linear transfer components are observed in these residues and hence these are predominantly produced through ICF process. Experimentally measured most probable ranges $R_p(\exp)$ deduced from FRRD curves along with $R_p(theo)$ evaluated from code SRIM08 [5], for CF and ICF components for each residues in the ^{20}Ne + ^{159}Tb system at ~ 164 MeV are listed in Table 3.4.

Broadening in the peaks observed in the forward recoil range distribution (FRRD) measurement is present because of the two reasons (i) straggling effect due to recoil velocity distribution of the evaporation residues (ii) particle(s) emission in the production of the residues. An attempt has been made to separate out the relative contribution of the CF and ICF of the residues produced in present measurements by fittings of the FRRD data with Gaussian peaks by using the ORIGIN software . The yield curves of evaporation residues obtained from FRRDs are assumed to be Gaussian in nature and may be given as [6, 7]:

$$Y = Y_0 + \frac{A}{\sqrt{2\pi\ \omega_A^2}} \exp\left[-\frac{(R-R_P)^2}{2\omega_A^2}\right] \qquad \ldots\ldots\ldots\ldots (3.1)$$

where R_P is the most probable mean range, ω_A is the width parameter (FWHM) of the recoil range distribution and A is the area under the peak. Further, the normalized yield Y may be estimated by the chi-square (χ^2) fit, from the experimentally determined

Table 3.4 The experimentally measured forward recoil ranges $R_p(\exp)$ deduced from RRD curves, and theoretically calculated most probable ranges $R_p(theo)$ for CF and /or ICF component using range energy relation for the reaction products produced in the interaction of ^{20}Ne with ^{159}Tb at energy, E ~ 164 MeV.

Residues	$R_p(\exp)$ **[µg/cm^2] CF of ^{20}Ne**	$R_p(theo)$ **[µg/cm^2]CF of ^{20}Ne**	$R_p(\exp)$ **[µg/cm^2] ICF of ^{16}O**	$R_p(theo)$ **[µg/cm^2] ICF of ^{16}O**	$R_p(\exp)$ **[µg/cm^2] ICF of ^{12}C**	$R_p(theo)$ **[µg/cm^2] ICF of ^{12}C**	$R_p(\exp)$ **[µg/cm^2] ICF of ^{8}Be**	$R_p(theo)$ **[µg/cm^2] ICF of ^{8}Be**
^{174}W (p4n)	985 ± 105	970						
^{175}Ta (α)	---		924 ± 90	916				
^{173}Ta (α2n)	---		913 ± 70	916				
^{172}Ta (α3n)	1009 ± 75	970	904 ± 60	916				
^{173}Hf (αpn)	---		912 ± 87	916				
^{164}Yb (2αp6n)	---		907 ± 75	916	683 ± 80	651		
^{166}Tm (3αn)	---		905 ± 73	916	658 ± 88	651	432 ± 78	443
^{165}Tm (3α2n)	---		906 ± 68	916	663 ± 76	651	448 ± 64	443
^{163}Tm (3α4n)	---		903 ± 80	916	656 ± 76	651	440 ± 77	443

production yield at different catcher foil thicknesses. The value of the chi-square (χ^2) fit was minimized in this analysis using a non-linear least-square fit routine, keeping the width parameter (ω_A) and most probable mean range (R_P) of the evaporation residues as a free parameter.

In order to separate out the contributions of complete (CF) and incomplete fusion (ICF) channels, in ^{20}Ne + ^{159}Tb system, the areas under the composite peaks in experimentally observed forward recoil range distribution (FRRD) curves shown in Figs. 3.4-3.6 have been computed. The relative contributions of the CF and ICF components are obtained by dividing the area of the corresponding peak distribution by the total area under the observed composite RRD curve. The relative contribution of CF of ^{20}Ne with the target ^{159}Tb for the residues ^{174}W (p4n) is found to be 100%. For the evaporation residues ^{175}Ta, ^{173}Ta and ^{172}Ta as shown in Figs. 3.4(b)-(d), the relative contributions of the ICF of the projectile ^{20}Ne by the fusion of the fragment ^{16}O with the target is found to be ~ 100%, ~ 100% and ~ 84% respectively. No CF contribution has been obtained for ^{175}Ta and ^{173}Ta while for the residue ^{172}Ta, its CF contribution is found to be ~ 16%. Similarly, for the evaporation residue ^{173}Hf , as shown in Figs.3.5(a), the relative contributions of the ICF of the projectile ^{20}Ne by the fusion of the fragment ^{16}O with the target is found to be ~ 100% while no CF contribution has been obtained. As such the residue ^{164}Yb is also produced via ICF with fusion of fragment ^{16}O and fusion of fragment ^{12}C. Their contributions are found to be 62% and 38% respectively. It is worth to mention here that our FRRD findings are supported by excitation function (EF) measurements as discussed in Chapter 2.

The relative contribution of ICF of fragment ^{16}O, ^{12}C and ^{8}Be for ^{166}Tm are found to be 32%, 42% and 26% respectively. While for ^{165}Tm, the relative contribution of ICF of fragment ^{16}O, ^{12}C and ^{8}Be are found to be 42%, 36% and 22% respectively. Moreover, the relative contribution of ICF of fragment ^{16}O, ^{12}C and ^{8}Be for the residue ^{163}Tm are found to be ≈ 38%, ≈ 34% and 28% respectively while the CF contributions of

the thulium isotopes are found to be negligible. The above description clearly indicates that depending upon the degree of linear momentum transfers (LMT). As such the relative contributions of CF and ICF channels for each residue have been estimated and are listed in Table 3.5. An attempt has been made to estimate the experimentally measured most probable ranges $R_p(\exp)$ and theoretically estimated forward mean ranges $R_p(theo)$ for all residues populated in CF and/or ICF components using code SRIM08 [5], based on range-energy relation for the reaction products at projectile energy ~164 MeV and are given in Table 3.4. As can be observed from this table, the experimentally measured most probable ranges for CF and ICF components agree well with theoretical ones within the experimental uncertainties.

Table 3.5 The measured relative contribution of CF and/or ICF of the reaction residues populated in ^{20}Ne + ^{159}Tb system at energy, E ~164 MeV.

Residue	**CF of ^{20}Ne**	**ICF of ^{20}Ne**		
		Fusion of fragment ^{16}O	**Fusion of fragment ^{12}C**	**Fusion of fragment ^{8}Be**
^{174}W (p4n)	100%	--	--	--
^{175}Ta (α)	--	100%	--	--
^{173}Ta (α2n)	--	100%	--	--
^{172}Ta (α3n)	16%	84%	--	--
^{173}Hf (αpn)	--	100%	--	--
^{164}Yb (2αp6n)	--	62%	38%	--
^{166}Tm (3αn)	--	32%	42%	26%
^{165}Tm (3α2n)	--	42%	36%	22%
^{163}Tm (3α4n)	--	38%	34%	28%

3.2.2 Forward recoil range distributions: $^{16}O + ^{156}Gd$ system

Forward recoil range distributions (FRRDS) for eight radio-nuclides ^{168}Hf (4n), ^{167}Lu (p4n), ^{167}Yb (αn), ^{162}Yb (α6n), ^{165}Tm (αp2n), ^{163}Tm (αp4n), ^{159}Ho^{g} (2αp4n) and ^{157}Dy (3α3n), populated in the interaction of ^{16}O with ^{156}Gd target have been measured at three different projectile energies ~ 72, ~ 82 and ~ 93 MeV. The normalized yields for these residues to obtain FRRDs, have been generated as a function of cumulative catcher thicknesses for each residues at the above three projectile energies. These are listed in Tables 3.6-3.10 and displayed in Fig. 3.7-3.14.

Table 3.6 Experimentally measured forward recoil range distributions (FRRDs) of the residues ^{168}Hf, ^{167}Lu, ^{167}Yb, ^{162}Yb, ^{165}Tm and ^{163}Tm produced in ^{16}O + ^{156}Gd reactions at ~72 MeV energy.

Cumulative thickness (μg/cm^2)	**Recoil range distributions (yields) of the residues measured in [mb/(mg/cm^2)]**					
	^{168}Hf	**^{167}Lu**	**^{167}Yb**	**^{162}Yb**	**^{165}Tm**	**^{163}Tm**
43.0	25.0	35.0	4.0		12.0	12.0
90.9	25.0	33.0	4.0	23.0	11.2	11.0
150.5	25.2	32.0	5.0	21.6	11.0	11.8
206.5	19.6	27.0	13.0	20.0	12.3	12.0
256.1	24.2	31.0	44.0	37.0	35.0	35.0
319.3	37.0	41.0	57.0	58.0	47.0	48.0
388.8	75.0	77.0	30.0	31.0	26.0	35.0
458.3	65.0	70.0	18.0	16.0	24.0	16.0
537.2	34.0	38.0	6.0	18.0	14.0	13.0
591.1	17.2	30.0	4.0	14.1	13.5	10.0
644.1	18.0	35.0	4.0	21.5	13.0	11.0
694.1	---	---	---	---	---	12.0
742.1	---	---	---	---	---	---
785.1	---	---	---	---	---	---
831.5	---	---	---	---	---	---

Table 3.7 Experimentally measured forward recoil range distributions (FRRDs) of the residues ^{168}Hf, ^{167}Lu, ^{167}Yb and ^{162}Yb produced in ^{16}O + ^{156}Gd reactions at ~82 MeV energy.

Cumulative thickness ($\mu g/cm^2$)	**Recoil range distributions (yields) of the residues measured in [mb/(mg/cm^2)]**			
	^{168}Hf	**^{67}Lu**	**^{167}Yb**	**^{162}Yb**
43.0	20.0	84.1	25.6	60.0
86.0	21.7	75.0	28.0	62.0
129.1	21.0	81.0	30.0	60.0
175.5	20.3	80.0	32.0	61.0
235.0	21.3	85.0	34.0	65.0
285.0	19.0	82.0	60.0	75.0
369.4	33.0	135.0	83.0	102.0
457.1	54.0	215.0	44.0	71.0
500.1	50.0	185.0	42.0	62.0
543.2	35.0	114.0	35.0	61.0
583.2	22.0	79.0	27.0	57.0
623.2	16.7	75.0	27.5	60.0
665.2	---	76.3	---	65.0
708.2	---	69.0	---	61.0
751.2	---	79.0	---	60.0
791.2	---	---	---	60.0

The disentangling of CF and ICF reaction products have been done in terms of full and partial linear momentum transfers (LMT) from projectile to target nucleus. The forward recoil range distribution of ^{168}Hf and ^{167}Lu populated via (4n) and (p4n) emission channels from equilibrated compound system ^{172}Hf*, at the above mentioned three projectile energies are shown in Figs. 3.7 (a)-(c) and Figs. 3.8(a)-(c) respectively.

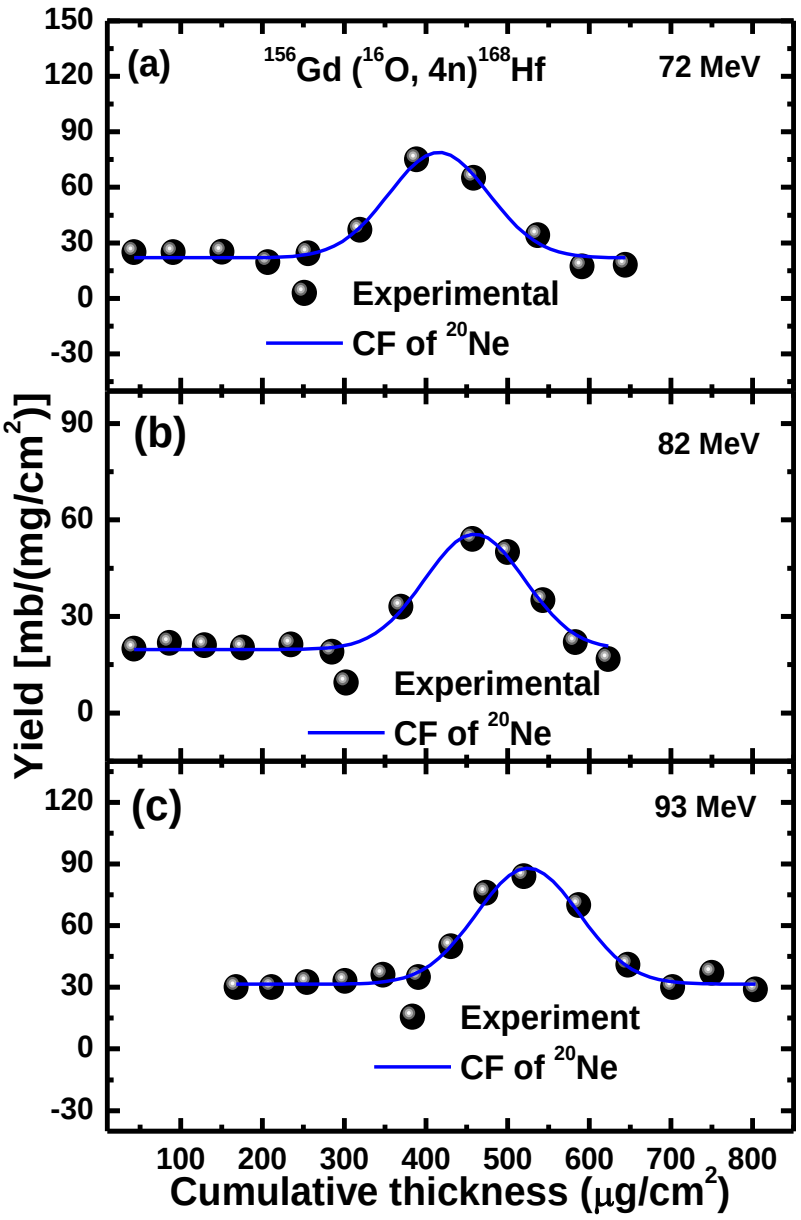

Fig. 3.7: The experimentally measured forward recoil range distributions (FRRDs) of evaporation residue ^{168}Hf, produced via CF, for ^{16}O + ^{156}Gd system at three different energies, E ~72, 82 and 93 MeV.

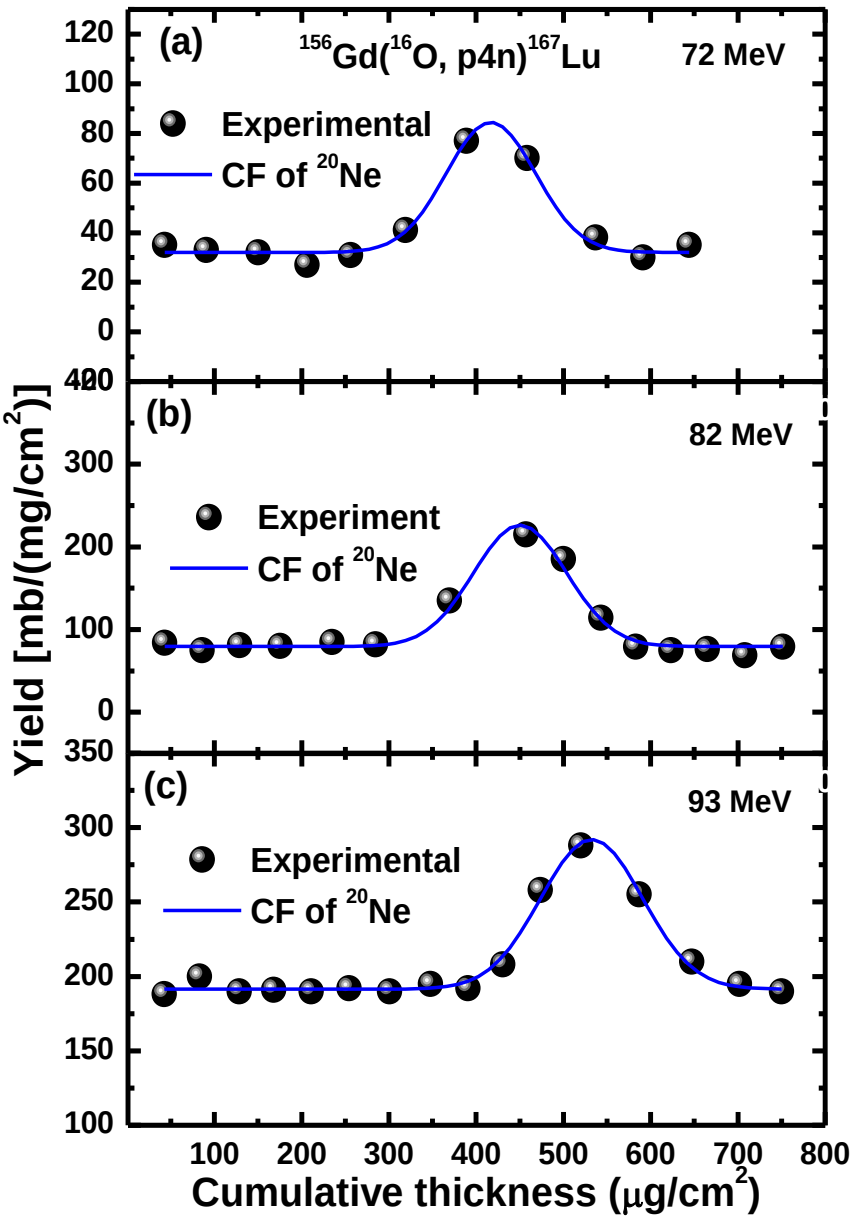

Fig. 3.8: The experimentally measured forward recoil range distributions (FRRDs) of evaporation residue ^{167}Lu, produced via CF, for ^{16}O + ^{156}Gd system at three different energies, E ~72, 82 and 93 MeV.

Table 3.8 Experimentally measured forward recoil range distributions (FRRDs) of the residues ^{165}Tm, ^{163}Tm, ^{159}Ho^{g} and ^{157}Dy produced in ^{16}O + ^{156}Gd reactions at ~82 MeV energy.

Cumulative thickness (μg/cm^2)	**Recoil range distributions (yields) of the residues measured in [mb/(mg/cm^2)]**			
	^{165}Tm	**^{163}Tm**	**^{159}Ho^{g}**	**^{157}Dy**
43.0	12.1	24.0	---	4.5
86.0	13.5	24.0	8.0	9.7
129.1	11.7	23.0	8.0	20.0
175.5	13.7	25.0	14.0	15.0
235.0	13.2	24.8	24.0	25.0
285.0	19.0	39.0	21.0	21.0
369.4	40.0	75.0	32.0	27.0
457.1	27.0	39.0	14.0	9.0
500.1	21.0	28.0	8.0	5.3
543.2	15.0	25.0	7.0	4.4
583.2	13.0	26.0	8.0	4.6
623.2	13.0	25.0	7.0	4.5
665.2	11.4	---	---	4.7
708.2	13.9	---	---	---
751.2	12.7	---	---	---
791.2	---	---	---	---

Table 3.9 Experimentally measured forward recoil range distributions (FRRDs) of the residues ^{168}Hf, ^{167}Lu, ^{167}Yb and ^{162}Yb produced in ^{16}O + ^{156}Gd reactions at ~93 MeV energy.

Cumulative thickness (μg/cm^2)	**Recoil range distributions (yields) of the residues measured in [mb/(mg/cm^2)]**			
	^{168}Hf	**^{167}Lu**	**^{167}Yb**	**^{162}Yb**
42.8	---	188.0	66.0	146.0
83.1	---	200.0	68.0	145.0
128.8	---	190.0	66.0	147.0
168.0	30.0	191.0	65.0	141.0
211.2	30.0	189.9	70.0	130.0
254.4	32.4	192.0	76.0	127.0
301.0	33.0	190.0	117.0	150.0
347.6	36.0	195.0	150.0	233.0
390.8	35.0	192.1	155.0	309.0
430.8	50.0	208.0	138.0	231.0
473.8	76.0	258.0	104.0	170.0
520.1	84.0	288.0	101.0	144.0
587.1	70.0	255.0	90.0	145.0
647.3	41.0	210.0	77.0	145.0
702.0	30.0	195.0	68.0	148.0
750.6	37.0	190.0	69.0	---
803.4	29.0	---	66.0	---
853.4	---	---	66.0	---
903.4	---	---	---	---

Table 3.10 Experimentally measured forward recoil range distributions (FRRDs) of the residues ^{165}Tm, ^{163}Tm, ^{159}Ho^{g} and ^{157}Dy produced in ^{16}O + ^{156}Gd reactions at ~93 MeV energy.

Cumulative thickness (μg/cm^2)	**Recoil range distributions (yields) of the residues measured in [mb/(mg/cm^2)]**			
	^{165}Tm	**^{163}Tm**	**^{159}Ho^{g}**	**^{157}Dy**
42.8	22.0	34.0	---	9.0
83.1	21.0	33.0	---	14.0
128.8	23.4	35.0	18.0	21.0
168.0	21.2	33.0	15.0	17.0
211.2	17.8	37.0	68.0	12.0
254.4	21.0	32.0	109.0	15.0
301.0	26.0	70.0	88.0	12.0
347.6	60.0	130.0	98.0	12.0
390.8	113.2	209.0	125.0	15.0
430.8	107.0	215.0	89.0	12.0
473.8	73.0	117.0	36.0	8.0
520.1	75.0	35.0	18.0	8.0
587.1	32.0	40.0	17.0	8.0
647.3	31.0	38.0	15.0	7.5
702.0	25.0	27.0	---	7.3
750.6	26.0	30.0	---	---
803.4	---	---	---	---
853.4	---	---	---	---
903.4	---	---	---	---

It can be observed from these figures that measured forward recoil range distributions (FRRDs) show only single Gaussian peak at each of the above three projectile energies, corresponding to full linear momentum transfer (LMT) from projectile to target nucleus. The experimentally measured most probable ranges $R_p(\exp)$ of CF channels along with theoretically estimated forward mean ranges $R_p(theo)$ using code SRIM08 [5] at ~ 72, ~ 82 and ~ 93 MeV energies are given in Tables 3.11-3.12. The agreement between experimental and theoretical ranges of these ERs revealed that the residues ^{168}Hf and ^{167}Lu are formed via CF of the projectile with the target nucleus, where entire LMT gets transferred from projectile to target nucleus. It is also observed from the Figs. 3.7 (a)-(c) and Figs. 3.8(a)-(c) that the mean peak positions of these residues, involved in CF process, shifts towards higher cumulative catcher thickness as the projectile energy increases, it is simply because LMT increases with projectile energy. Further it may be pointed out that nucleons emission from the composite system may little change energy and momentum of the recoiling nucleus, depending upon the direction of emission, which may be reflect in FWHM of the Gaussian shaped recoil range distributions of these residues.

On the other hand, the recoil range distribution of the residue ^{167}Yb populated in the interaction of ^{16}O with ^{156}Gd target at three energies are shown in Figs. 3.9(a)-(c). It can be observed from Figs 3.9(a)-(c) that FRRDs of residue ^{167}Yb have two peaks structure, one corresponds to full LMT components (i.e., due to fusion of projectile ^{16}O) and another corresponds to partial LMT components (i.e., due to fusion of fragment ^{12}C) with ^{156}Gd. The observed peaks corresponding to full LMT (i.e., in fusion of projectile ^{16}O) at cumulative catcher thicknesses ~ 406, ~ 475 and ~ 536 μg/cm^2 at three different projectile energies i.e., ~ 72, ~ 82 and ~ 93 MeV, while another peak corresponding to partial LMT transfer (i.e., in fusion of fragment ^{12}C) at cumulative Al-catcher foil thicknesses ~ 297, ~ 342 and ~ 380 μg/cm^2 at the same projectile energies as above. Peaks corresponding to full and partial LMT reveals that the reaction product may be

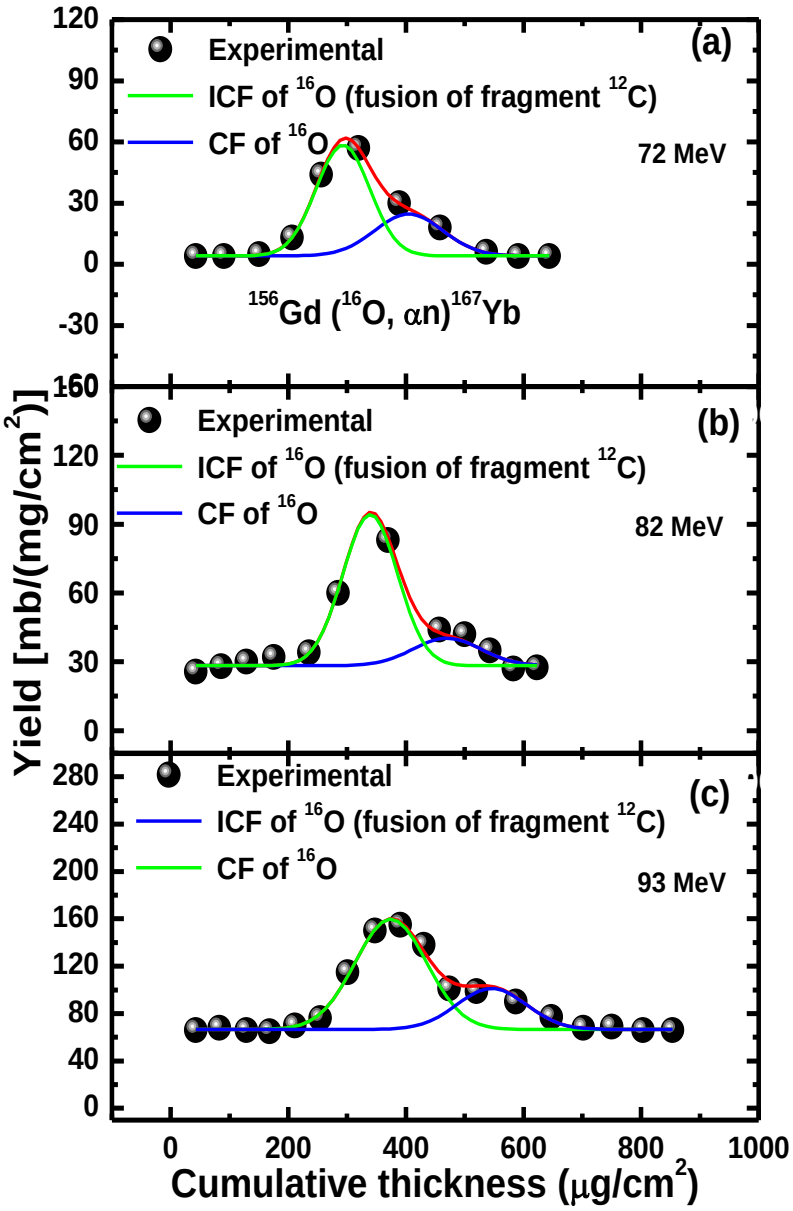

Fig. 3.9: The experimentally measured forward recoil range distributions (FRRDs) of evaporation residue ^{167}Yb, produced via CF and ICF, for ^{16}O + ^{156}Gd system at three different energies, E ~72, 82 and 93 MeV.

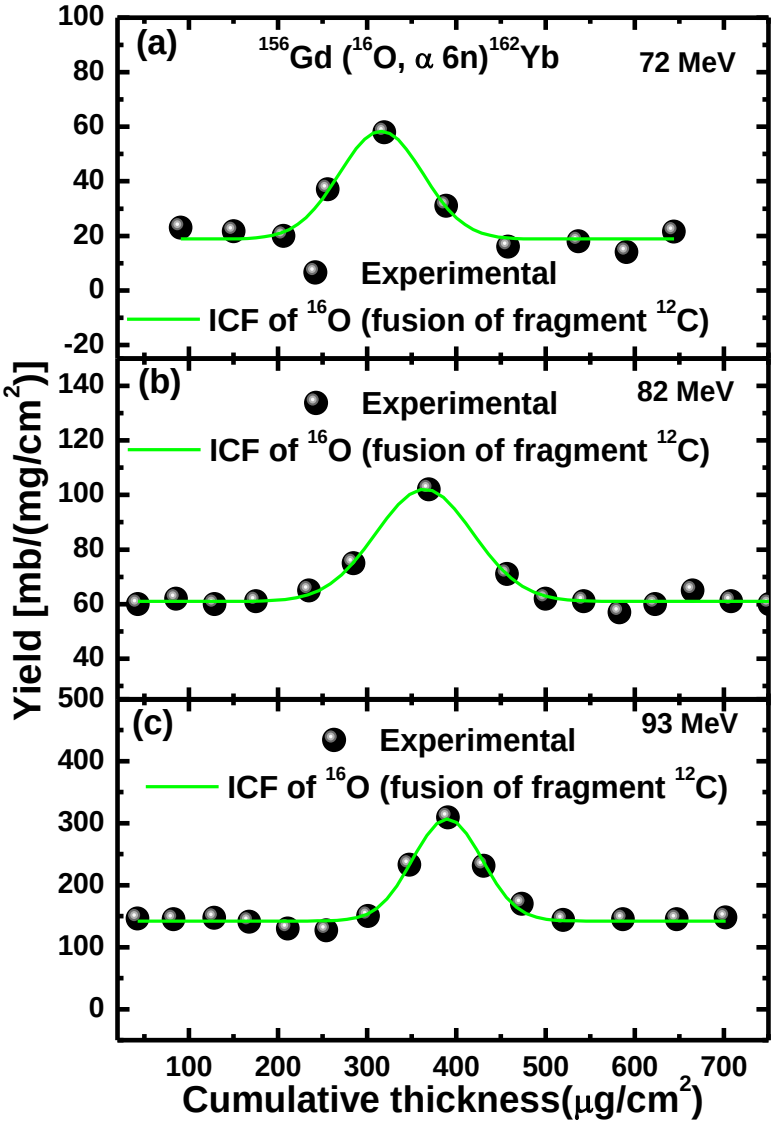

Fig. 3.10: The experimentally measured forward recoil range distributions (FRRDs) of evaporation residue ^{162}Yb, produced via ICF, for ^{16}O + ^{156}Gd system at three different energies, E ~72, 82 and 93 MeV.

populated via CF and ICF both. The reaction product ^{167}Yb populated corresponding to full LMT (i.e., in fusion of ^{16}O) with target ^{156}Gd and may be explained by assuming that incoming projectile ^{16}O captured by the target nucleus ^{156}Gd and compound nucleus ^{172}Hf* is formed, which de-excites via emission of one α-particle and one neutron leadingto the production of residue ^{167}Yb. The same residue may also be populated in partial LMT (i.e., in fusion of fragment ^{12}C) with the target ^{156}Gd, which may be explained by assuming projectile ^{16}O break-up of into ^{12}C and ^{4}He (α-particle) followed by the fusion of ^{12}C with ^{156}Gd, forming an incompletely fused composite system ^{168}Yb*. It de-excites by the emission of one neutron. The break-up α-particle fragment moves in the forward direction without any interaction with target nucleus as a spectator. It may also be observed from the Figs. 3.9(a)-(c) that experimentally measured most probable ranges $R_p(\exp)$ shifts towards higher cumulative thickness as projectile energy increases as expected. Hence, it may be inferred that residue ^{167}Yb has contributions coming from both CF and ICF.

Further, the forward recoil range distributions (FRRDs) of residue ^{162}Yb at the above three energies are displayed in Figs. 3.10(a)-(c). It can be observed from each figure that there is only single peak at cumulative catcher thickness ~ 312, ~ 362 and ~390 μg/cm^2 at projectile energies ~ 72, ~ 82 and ~ 93 MeV respectively. It may however be pointed out that the partial LMT component at relatively smaller cumulative thickness may be associated with ICF of ^{16}O (in the fusion of fragment ^{12}C) with target nucleus ^{156}Gd. The composite system ^{168}Yb* may decay by the emission of six neutrons. It may also be observed that experimentally measured most probable ranges $R_p(\exp)$ agree well with theoretically calculated mean ranges (corresponds to fusion of fragment ^{12}C) and peak shifts towards higher cumulative catcher thickness as projectile energy increases as expected. It may therefore be inferred that the populated residue ^{162}Yb has contribution coming from the ICF process of the projectile only.

Furthermore, it can be visualized from Fig. 3.11(a)-(c) that the recoil range distributions curves of reaction product ^{165}Tm at three projectile energies show two Gaussian peaks, corresponding to two LMT components, one at mean recoil ranges (corresponding to the fusion of projectile ^{16}O) with the target, observed at ~ 418, ~ 456 and ~ 519 μg/cm^2 at three different projectile energies ~ 72, ~ 82 and ~ 93 MeV respectively, may be associated with CF of ^{16}O with ^{156}Gd target nucleus. While, other LMT component corresponding to lower mean recoil range or cumulative thicknesses (corresponding to the fusion of fragment ^{12}C produced in the break-up of the projectile) at ~ 300, ~359 and ~ 407 μg/cm^2 may be associated with ICF of the projectile at the respective energies. Thus, the residue ^{165}Tm is expected to be populated via CF as well as ICF processes. Similarly, the measured FRRD of evaporation residue ^{163}Tm has been plotted in Fig. 3.12(a)-(c). The reaction product ^{163}Tm is associated with only single LMT component (due to fusion of fragment ^{12}C) at mean recoil range ~ 322, ~ 366 and ~ 409 μg/cm^2 at ~ 72, ~ 82 and ~ 93 MeV energies corresponds to the fusion of fragment ^{12}C with target ^{156}Gd, leading to the formation of incompletely fused composite nucleus ^{168}Yb*, which de-excites by the emission of one proton and four neutrons. Hence, the residue ^{163}Tm is also expected to be populated via ICF of the projectile.

In the same way, FRRDs of reaction product ^{159}Ho^g [shown in Figs. 3.13(a) -(b)] has two peaks composite structure, one peak at cumulative thicknesses ~ 379 and ~ 388 μg/cm^2 corresponding to partial LMT component (due to the fusion of fragment ^{12}C with the target, in the projectile break-up) and other peak at cumulative catcher thicknesses ~ 230 and ~ 252 μg/cm^2 corresponding to partial LMT component (due to the fusion of fragment ^{8}Be in the projectile break-up) at projectile energies ~ 82 and ~ 93 MeV. It is quite clear that ^{159}Ho is also expected to be populated via ICF process.

Measured FRRDs for the radio-isotope ^{157}Dy at two projectile energies ~ 82 and 93 MeV are displayed in Fig. 3.14(a)-(b). It can be observed from these figures that composite distribution curves may be resolved into three Gaussian peaks involving three different LMT components. The first peaks are observed at partial LMT component

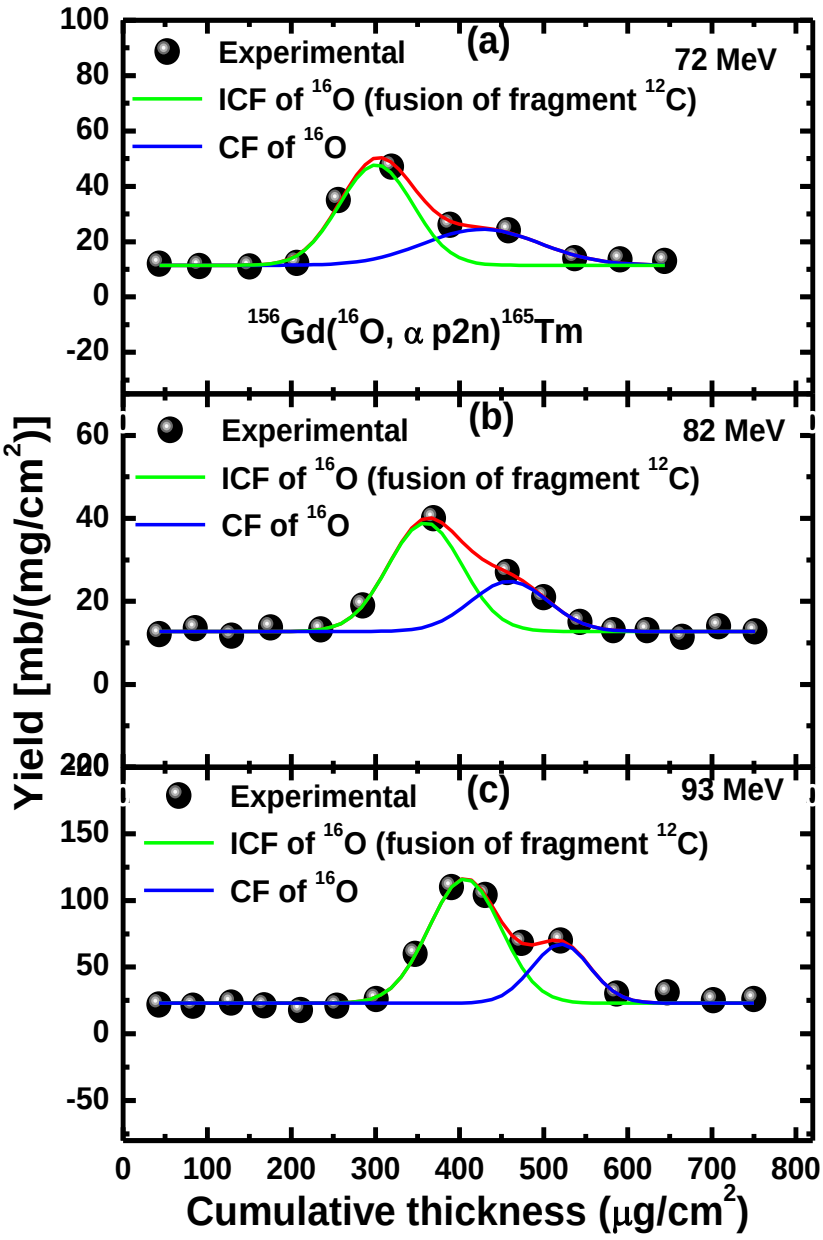

Fig. 3.11: The experimentally measured forward recoil range distributions (FRRDs) of evaporation residue ^{165}Tm, produced via CF and ICF, for ^{16}O + ^{156}Gd system at three different energies, E ~72, 82 and 93 MeV.

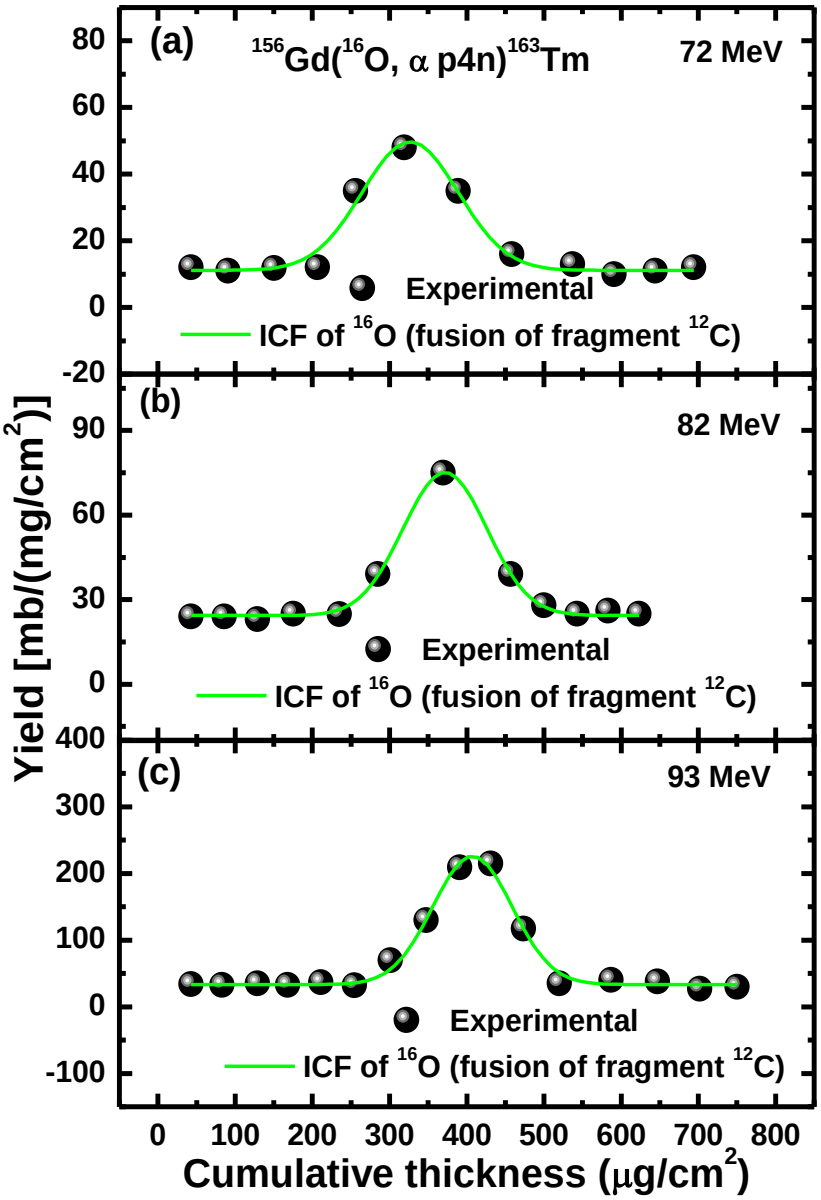

Fig. 3.12: The experimentally measured forward recoil range distributions (FRRDs) of evaporation residue ^{163}Tm, produced via ICF, for ^{16}O + ^{156}Gd system at three different energies, E ~72, 82 and 93 MeV.

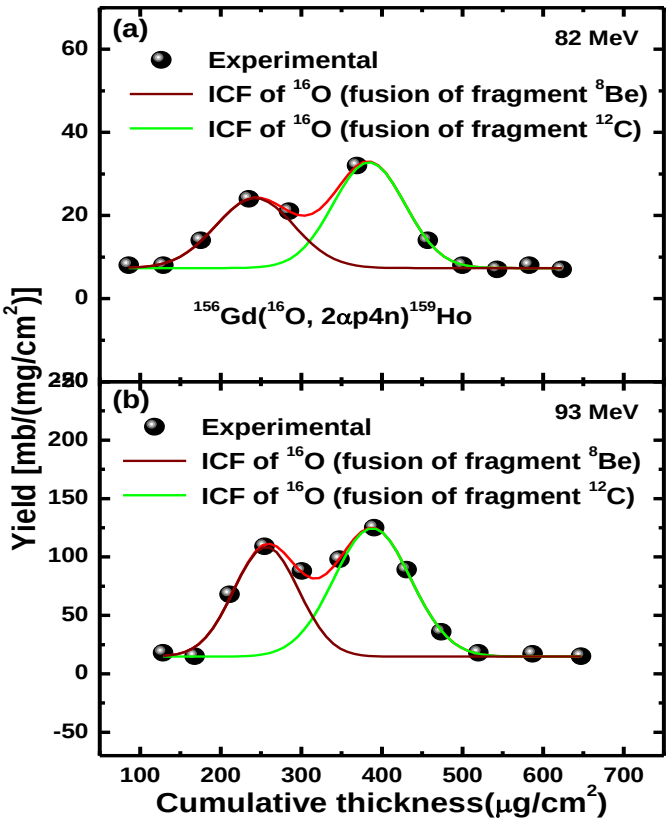

Fig. 3.13: The experimentally measured forward recoil range distributions (FRRDs) of evaporation residue ^{159}Ho^{g}, produced via ICF, for ^{16}O + ^{156}Gd system at two different energies, E ~ 82 and 93 MeV.

corresponding to cumulative catcher thicknesses ≈ 357 and 400 μg/cm^2 associated with ICF of the projectile ^{16}O (due to fusion of fragment ^{12}C), at ~ 82 and 93 MeV energy respectively. The second peak is observed at partial LMT component corresponding to cumulative catcher thicknesses ~ 230 and 263 μg/cm^2 associated with ICF of the projectile ^{16}O (due to fusion of fragment ^{8}Be), while the third peaks at each energy is observed again at partial LMT component corresponding to cumulative catcher thicknesses ~ 121 and 127 μg/cm^2 associated with ICF of the projectile ^{16}O (due to fusion of fragment ^{4}He) with the target. No peaks are observed corresponding to full

LMT in the FRRD curves. As such, it can be inferred that this residue ^{157}Dy is populated through ICF reaction process. It is worth to mention that experimentally measured forward recoil ranges for each LMT components associated with the residues are generally in good agreement with theoretically estimated most probable mean ranges calculated using code SRIM08 [5] , with in experimental uncertainties, as has been shown in Tables 3.11-3.12. The errors shown with R_p(exp) are the FWHM of the Gaussian distribution of the experimental values.

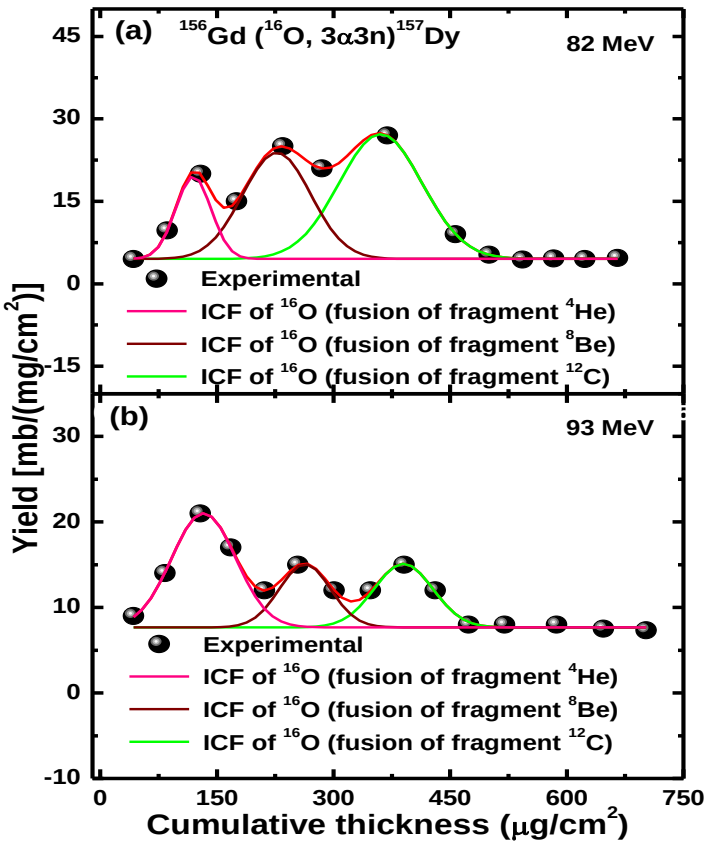

Fig. 3.14: The experimentally measured forward recoil range distributions (FRRDs) of evaporation residue ^{157}Dy, produced via ICF, for ^{16}O + ^{156}Gd system at two different energies, E ~ 82 and 93 MeV.

Table 3.11 The experimentally measured forward recoil ranges $R_p(\exp)$ deduced from RRD curves, and theoretically calculated most probable ranges $R_p(theo)$ for CF and /or ICF component using range energy relation for the reaction products produced in the interaction of ^{16}O with ^{156}Gd at energy, E ~ 72 and 82 MeV.

Residues	$R_p(\exp)$ **[μg/cm²] CF of ^{16}O**	$R_p(theo)$ **[μg/cm²] CF of ^{16}O**	$R_p(\exp)$ **[μg/cm²] ICF of ^{12}C**	$R_p(theo)$ **[μg/cm²] ICF of ^{12}C**	$R_p(\exp)$ **[μg/cm²] ICF of ^{8}Be**	$R_p(theo)$ **[μg/cm²] ICF of ^{8}Be**	$R_p(\exp)$ **[μg/cm²] ICF of ^{4}He**	$R_p(theo)$ **[μg/cm²] ICF of ^{4}He**
E ~ 72 MeV								
^{168}Hf (4n)	412 ± 61	403						
^{167}Lu (p4n)	416 ± 53	403						
^{167}Yb (αn)	406 ± 58	403	297 ± 45	305				
^{162}Yb (α6n)	---		312 ± 47	305				
^{165}Tm (αp2n)	418 ± 69	403	300 ± 43	305				
^{163}Tm (αp4n)	---		322 ± 62	305				
E ~ 82 MeV								
^{168}Hf (4n)	456 ± 61	459						
^{167}Lu (p4n)	450 ± 58	459						
^{167}Yb (αn)	475 ± 57	459	342 ± 46	351				
^{162}Yb (α6n)	---		362 ± 55	351				
^{165}Tm (αp2n)	456 ± 45	459	359 ± 44	351				
^{163}Tm (αp4n)	---		366 ± 54	351				
^{159}Ho^{g} (2αp4n)	---		379 ± 44	351	230 ± 48	235		
^{157}Dy (3α3n)	---		357 ± 53	351	230 ± 44	235	121 ± 23	117

Table 3.12 The experimentally measured forward recoil ranges $R_p(\exp)$ deduced from RRD curves, and theoretically calculated most probable ranges $R_p(theo)$ for CF and / or ICF component using range energy relation for the reaction products produced in the interaction of ^{16}O with ^{156}Gd at energy, E ~ 93 MeV.

Residues	$R_p(\exp)$ **[µg/cm^2] CF of ^{16}O**	$R_p(theo)$ **[µg/cm^2] CF of ^{16}O**	$R_p(\exp)$ **[µg/cm^2] ICF of ^{12}C**	$R_p(theo)$ **[µg/cm^2] ICF of ^{12}C**	$R_p(\exp)$ **[µg/cm^2] ICF of ^{8}Be**	$R_p(theo)$ **[µg/cm^2] ICF of ^{8}Be**	$R_p(\exp)$ **[µg/cm^2] ICF of ^{4}He**	$R_p(theo)$ **[µg/cm^2] ICF of ^{4}He**
E ~ 93 MeV								
^{168}Hf (4n)	519 ± 66	521						
^{167}Lu (p4n)	527 ± 58	521						
^{167}Yb (αn)	536 ± 59	521	380 ± 61	397				
^{162}Yb (α6n)	---		390 ± 38	397				
^{165}Tm (αp2n)	519 ± 35	521	407 ± 43	397				
^{163}Tm (αp4n)	---		409 ± 51	397				
^{159}Ho^{g} (2αp4n)	---		388 ± 48	397	252 ± 40	268		
^{157}Dy (3α3n)	---		400 ± 38	397	263 ± 33	268	127 ± 41	

In the present work, an attempt has been made to deduce the relative contributions of CF and ICF for various ERs from the measured FRRDs for ^{16}O + ^{156}Gd system at three different projectile energies ~ 72, ~82 and ~ 93 MeV and are listed in Table 3.13. The relative contributions the residues ^{168}Hf (4n) and ^{167}Lu (p4n) produced in

CF of the projectile with target is found to be 100% at each projectile energy. Reaction product ^{167}Yb(αn) is populated via CF as well as ICF (in the fusion the fragment ^{12}C with the target ^{156}Gd) is found to have (33 % and 67 %), (18% and 82%) and (27% and 73%) contributions for CF and ICF at 72, 82 and 93 MeV energies respectively. Residue ^{162}Yb (α6n) is expected to be produced only via ICF of the projectile, where in the fusion of the fragment ^{12}C (which is produced in the projectile break-up) takes place with the target. Hence, it has 100% ICF contribution at each energy. As such, the residue ^{165}Tm (αp2n) is again found to be produced of via both CF and ICF (in the fusion of fragment ^{12}C) at each projectile energy. The contributions of CF and ICF are obtained to be (36% and 64%), (32% and 68%) and (28% and 72%). The ICF contribution is also found to increase with projectile energy while CF contribution decreases with energy. The residue ^{163}Tm (αp4n) is also produced 100% via ICF only (in the fusion of fragment ^{12}C). The evaporation residue ^{159}Ho^{g} (2αp4n) is expected to be produced by two modes of ICF. First in the fusion of the fragment ^{12}C with the target and second in the fusion of fragment ^{8}Be with the target, if it is assumed that the projectile ^{16}O breaks-up into ^{12}C+ ^{4}He and/or ^{8}Be+ ^{8}Be (2α) fragments when reaches in the nuclear field. There contributions are obtained to be (58% and 42%) and (60% and 40%) at 82 and 93 MeV energies respectively. As such, the residue ^{157}Dy (3α3n) is expected to be produced by three modes of ICF i.e., fusion of the fragment ^{12}C; fusion of fragment ^{8}Be and fusion of fragment ^{4}He, with target ^{156}Gd (in the projectile break-up). Their contributions are estimated to be (51%, 35%, 14%) and (21%, 25%, 54%) respectively, at 82 and 93 MeV projectile energies. The relative contributions of ICF of the projectile ^{16}O (due to the fusion of fragment ^{12}C, ^{8}Be and ^{4}He) have been found for ^{157}Dy.

Table 3.13 The measured relative contribution of CF and/or ICF of the reaction products populated in ^{16}O + ^{156}Gd system at three different projectile energies i.e., E ~ 72, 82 and 93 MeV.

Residues	Energy (MeV)	CF of ^{16}O (%)	ICF of ^{16}O		
			Fusion of fragment ^{12}C (%)	Fusion of fragment ^{8}Be (%)	Fusion of fragment ^{4}He (%)
^{168}Hf (4n)	72	100	--	---	---
	82	100	---	---	---
	93	100	---	---	---
^{167}Lu (p4n)	72	100	---	---	---
	82	100	---	---	---
	93	100	---	---	---
^{167}Yb (αn)	72	33	67	---	---
	82	18	82	---	---
	93	27	73	---	---
^{162}Yb (α6n)	72	---	100	---	---
	82	---	100	---	---
	93	---	100	---	---
^{165}Tm (αp2n)	72	36	64	---	---
	82	32	68	---	---
	93	28	72	---	---
^{163}Tm (αp4n)	72	---	100	---	---
	82	---	100	---	---
	93	---	100	---	---
$^{159}Ho^{g}$(2 αp4n)	82	---	58	42	---
	93	---	60	40	---
^{157}Dy(3α3n)	82	---	51	35	14
	93	---	21	25	54

It can be observed from the Table 3.13 that break-up of the projectile ^{16}O takes place in the nuclear field in the form of cluster (s) of α–particles and ICF channels are opened. Moreover, it is also observed that ICF contribution increases with projectile energy in general.

References:

[1] MAESTRO; Data acquisition and analysis software coupled with EG & G ORTEC Hardware., U.S.A.

[2] FREEDOM; Data acquisition and analysis software, designed to support the accelerator based experiments at the Inter-University Accelerator Centre (IUAC), New Delhi, India.

[3] E. Brown and R. B. Firestone; *Table of Radioactive Isotopes*, Wiley, New York, 1986.

[4] J. K. Tuli; Nuclear Wallet Card, National Nuclear Data Centre, Brookhaven National Laboratory, Upton, New York, USA-2000.

[5] J. F. Ziegler; **SRIM08**, *The Stopping Power and Range of Ions in Matter, 2008* http://www.srim.org

[6] G. N. Simonoff and J. M. Alexander, Phys. Rev. **133** (1964) B104.

[7] P. P. Singh, M. K. Sharma, Unnati, D. P. Singh, R. Kumar, K. S. Golda, B. P. Singh and R. Prasad; Eur. Phys. J. A **34** (2007) 29.